

RESEARCH ARTICLE | AUGUST 21 2018

Superconducting radio-frequency virtual cavity for control algorithms debugging ^{EP}

Pablo Echevarria ^{ID} ; Eukeni Aldekoa; Josu Jugo ^{ID} ; Axel Neumann; Andriy Ushakov; Jens Knobloch



Rev. Sci. Instrum. 89, 084706 (2018)

<https://doi.org/10.1063/1.5041079>



View
Online



Export
Citation

CrossMark

Articles You May Be Interested In

Software Reliability Modeling Incorporating Log-Logistic Testing-Effort with Imperfect Debugging

AIP Conference Proceedings (October 2010)

Application of advanced micromachining techniques for the characterization and debug of high performance microprocessors

J. Vac. Sci. Technol. B (January 1999)

Cryogenic system for BERLinPro

AIP Conference Proceedings (January 2014)

500 kHz or 8.5 GHz?
And all the ranges in between.

Lock-in Amplifiers for your periodic signal measurements



Find out more



Superconducting radio-frequency virtual cavity for control algorithms debugging

Pablo Echevarria,^{1,a)} Eukeni Aldekoa,² Josu Jugo,² Axel Neumann,¹ Andriy Ushakov,¹ and Jens Knobloch^{1,3}

¹Helmholtz Zentrum Berlin, Albert Einstein Strasse 15, 12489 Berlin, Germany

²University of the Basque Country UPV/EHU, Leioa, Bizkaia, Spain

³Department of Physics, Universität Siegen, 57068 Siegen, Germany

(Received 23 May 2018; accepted 29 July 2018; published online 21 August 2018)

Superconducting radio-frequency (SRF) cavities are one of the most important elements in modern particle accelerators as they are used for beam acceleration, bunch manipulation, bunch focusing and defocusing, etc. Nevertheless, the availability of these complex structures prior to their installation in the accelerator is limited, either due to a lack of a real cavity or due to the time needed for the experiment setup (vacuum, cryogenics, cabling, etc.), and thus it can block or delay the development of new algorithms such as low level RF control, quench detection, etc. In this paper, we present a hardware virtual cavity to be used in hardware-in-the-loop simulations. The system implements a cavity electrical model for the transmitted and reflected voltages and more advanced features such as mechanical vibration modes driven by Lorentz-force detuning or external microphonics, hard quenches, and the Q-slope. As viewed from the RF input and output, this virtual cavity acts like a real SRF cavity and can replace such a system in early-stage debugging and operation of ancillary control systems. © 2018 Author(s). All article content, except where otherwise noted, is licensed under a Creative Commons Attribution (CC BY) license (<http://creativecommons.org/licenses/by/4.0/>). <https://doi.org/10.1063/1.5041079>

I. INTRODUCTION

The utilization of superconducting radio-frequency (SRF) cavities for particle acceleration is spreading not only in large scale accelerators like the LHC,¹ European XFEL,² or the LCLS-II,³ but also in smaller facilities like ELBE,⁴ MESA,⁵ BESSY-VSR,⁶ and bERLinPro.⁷ Regardless of the kind of facility that uses the SRF technology, the cavities are an extremely expensive item. Moreover, the equipment needed to test them, such as cryomodules with the subsequent cryogenic and ultra-high vacuum installation, the bunker for radiation protection, and a clean room for the proper cavities' manipulation, is not always available in the early stages of system development. Additionally once this equipment is installed, the time to test control algorithms is very limited. This lack of available time to use real cavities is a major drawback when designing control algorithms, such as low level RF control algorithms, microphonics compensation, and machine protection techniques.

A solution to overcome this issue is to perform hardware-in-the-loop simulations, i.e., to replace the actual cavity by an electronics system that mimics its behavior in terms of its response to a drive signal. This idea, very extended for the model-based development, was first proposed in Ref. 8, where the RF model with the detuning caused by three mechanical vibration modes was implemented in an Field Programmable Gate Array (FPGA) using Very High Speed Integrated Circuit Hardware Description Language (VHDL) code. In Ref. 9, the cavity equivalent circuit for the in-phase (I) and in-quadrature

(Q) base-band components was implemented in an FPGA. Both of these implementations are based on discontinued hardware; thus, their use and further developments are not possible.

In this work, a virtual cavity implemented in off-the-shelf National Instrument's hardware using the Labview visual programming interface is presented. As in Ref. 8, the RF model of the cavity is implemented in an FPGA, but in this case, five mechanical eigenmodes were included in addition to extra features such as the hard quenching of the cavity and the so-called Q-slope (i.e., the quality factor of the cavity depends on the amplitude of the RF field). The range of the cavity's parameters is wide and easily changed by the operator via a graphical user interface (GUI). For example, the resonance frequency of the cavity can vary from some hundreds of MHz to up to 1.75 GHz, making it possible to use the virtual cavity for modeling from Helmholtz Zentrum Berlin's (HZB) quadrupole resonator¹⁰ to a BESSY-VSR cavity.⁶ The range of quality factors and loaded quality factors of the cavity allows for the implementation of cavities ranging from under coupling to highly over coupled conditions, etc.

The organization of this work is as follows. In Sec. II, the electrical model of a SRF cavity is described and its implementation is presented in Sec. III. Section IV presents the additional features included in the virtual cavity such as quenches, field dependent Q_0 , and the mechanical resonance modes. Section V also presents the results on the dynamic transmitted and reflected voltages as a function of drive signal together with the results of quenches, the field dependent Q_0 , and mechanical vibrations features. Section VI explains the limitations of the virtual cavity and proposes future work to

^{a)}Electronic mail: pablo.echevarria@helmholtz-berlin.de

overcome them. Section VII shows the applications where this virtual cavity has already been used or is planned to be used. Finally some conclusions are given in Sec. VIII.

II. ELECTRICAL CAVITY MODEL

It is well known that a superconducting cavity can be modeled using an equivalent electric circuit¹¹ where the power amplifier and beam are represented as current generators, the fundamental power coupler as a transformer, and the cavity as an RLC-circuit. Figure 1 shows the equivalent circuit of the fundamental mode of a cavity connected to an RF power source, where V_{cav} represents the transmitted voltage to the cavity and V_{ref} represents the reflected voltage sent to the circulator in order to protect the RF power source. The circuit components are defined in terms of the cavity parameters

$$\sqrt{\frac{L}{C}} = R/Q, \quad (1)$$

$$\omega_0 = \frac{1}{\sqrt{LC}}, \quad (2)$$

$$R/Q = \frac{R_{\text{sh}}}{Q_0} = \frac{2R}{Q_0}. \quad (3)$$

In this case, R is the equivalent circuit resistance whose relationship to the shunt impedance is¹¹ $R_{\text{sh}} = 2R$ according to the accelerator physics definition. The ratio of the transformer, m , can be given in terms of coupling factor of the fundamental power coupler β , $m = \sqrt{\frac{R}{\beta Z_0}}$. The behavior of the RF envelope of the transmitted voltage without beam can be calculated by the following equation:

$$\frac{d}{dt} \mathbf{V}_{\text{cav}} = \begin{pmatrix} -\omega_{1/2} & -\Delta\omega \\ \Delta\omega & -\omega_{1/2} \end{pmatrix} \mathbf{V}_{\text{cav}} + \begin{pmatrix} R_L \omega_{1/2} & 0 \\ 0 & R_L \omega_{1/2} \end{pmatrix} \frac{\mathbf{I}_{\text{amp}}}{m} \quad (4)$$

with $\omega_{1/2} = \frac{\omega_0}{2Q_L}$, R_L being the load resistance, $R_L = \frac{R}{1+\beta}$, and $\Delta\omega$ being the difference between the driving frequency and the RF resonance frequency, $\Delta\omega = \omega_0 - \omega$. $\mathbf{V}_{\text{cav}} = (V_{\text{cav}}^r, V_{\text{cav}}^i)^T$ and $\mathbf{I}_{\text{amp}} = (I_{\text{amp}}^r, I_{\text{amp}}^i)^T$ are the real and imaginary parts of the cavity voltage and RF power source current, respectively. In order to be implemented in a digital device, this equation can

be discretized as follows:

$$\mathbf{V}_{\text{cav}}(k+1) = \left[T_s \begin{pmatrix} -\omega_{1/2} - \Delta\omega & \\ \Delta\omega & -\omega_{1/2} \end{pmatrix} + 1 \right] \mathbf{V}_{\text{cav}}(k) + \left[T_s \begin{pmatrix} R_L \omega_{1/2} & 0 \\ 0 & R_L \omega_{1/2} \end{pmatrix} \right] \frac{\mathbf{I}_{\text{amp}}}{m}, \quad (5)$$

where T_s is the sampling period and k is the time step. The calculation of the reflected voltage is done using

$$\mathbf{V}_{\text{ref}}(k) = \frac{\mathbf{V}_{\text{cav}}(k)}{m} - \frac{Z_0 \mathbf{I}_{\text{amp}}(k)}{2}. \quad (6)$$

III. DIGITAL IMPLEMENTATION

In order to do the hardware implementation, a commercial off the shelf device by National Instruments was chosen, which allows for easy sharing of the Labview code with other institutions. This device consists of a PXIe chassis,¹² a chassis controller running Windows,¹³ an FPGA module,¹⁴ and an analog adapter module.¹⁵

The signal of the RF module feeds one of the two inputs of the analog adapter module. Then this signal is sent to the FPGA module where it is sampled at a maximum sampling frequency of 100 MHz with 14 bit precision and fed to a Virtex-5 FPGA. The digitized signal is IQ-demodulated, and then, I and Q components are used as inputs for Eqs. (5) and (6) which are implemented in the FPGA. As the FPGA uses fixed point arithmetic, the input has to be converted into this numeric representation. The chosen decimal point is such that the maximum power at the input port (4 dBm) is converted into an I_{amp} with an amplitude of 8 A, which means an RF input of 3.2 kW.

The cavity parameters are sent to the FPGA module through the chassis back-plane by the Windows controller where an operator can insert them using a GUI. The possible parameters are Q_0 , Q_{ext} , R/Q , Δf , f_{RF} , and T_s , which are used to calculate the factors to be sent to the FPGA and some other parameters to be shown to the operator as $\beta = \frac{Q_0}{Q_{\text{ext}}}$, $Q_L = \frac{Q_0}{1+\beta}$, $T_{\text{fall}} = \frac{2Q_L}{\omega_0}$, $\omega_{1/2} = \frac{\omega_0}{2Q_L}$, etc.

Once \mathbf{V}_{cav} and \mathbf{V}_{ref} are calculated in the FPGA, they are IQ-modulated to reconstruct the original input's frequency. The user can select which variables are sent to the 16 bit DAC and therefore to the analog adapter module's outputs. The wide range of values of \mathbf{V}_{cav} and \mathbf{V}_{ref} can result in an output that is too low to be resolved for certain cavity parameter settings. In order to improve the dynamic range of the DAC, the user

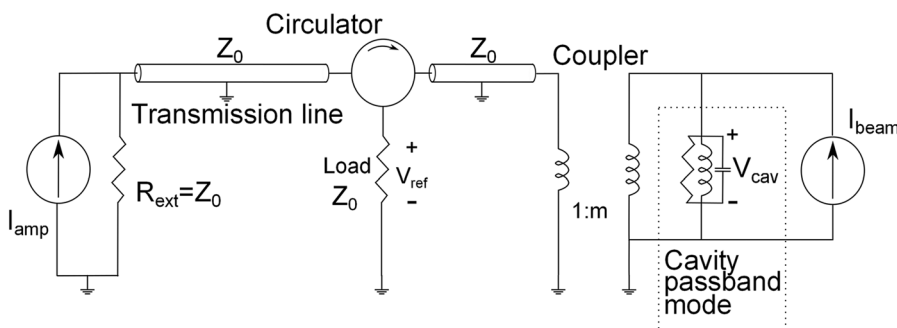


FIG. 1. Equivalent circuit model for a cavity accelerating a particle beam and connected via a coupler antenna to an RF power source.

can also do a digital shift to select which 16 bits of the internal representation of the signals are sent to the analog adapter module. The maximum possible V_{cav} is 67 MV due to the selected internal numeric representation.

IV. ADDING REALISTIC SRF RESONATOR PROPERTIES

In the presented virtual cavity, the block that implements the cavity model for the transmitted and reflected voltage [Eqs. (5) and (6)] in the FPGA gets, by default, the parameters from the Windows controller. But the Virtex-5 FPGA has enough resources to allow the implementation of some additional algorithms to include many real-life features of SRF cavities. These include field dependent quality factors, quench behavior, microphonics, and the cavity mechanical response as well as Lorentz-force detuning. Figure 2 shows the block diagram of the system, where the electrical model of the cavity gets the parameters directly from the controller or from the built-in blocks that implement the quenches, the field dependent Q, and the mechanical vibrations driven by Lorentz force detuning and external microphonics. The details of the implementation of these realistic behaviors are given in Subsections IV A–IV C.

A. Hard quench

Cavities can quench due to various mechanisms such as defect heating or H exceeding the critical field. As a result, the Q_0 of the cavity rapidly drops to a value typical of a normal conducting one. This process, known as hard quench, has been implemented in the FPGA.

The components V_{cav}^r and V_{cav}^i are used to calculate the amplitude of the voltage inside the cavity in real time, and if this value is above a threshold set by the operator in the GUI, the $\omega_{1/2}$ is set to the maximum allowed by the implementation which means $Q_0 \approx 175\,000$ for high Q_e at $f_{RF} = 1.3$ GHz (see Sec. VI). If the quench condition is met, it will not be possible

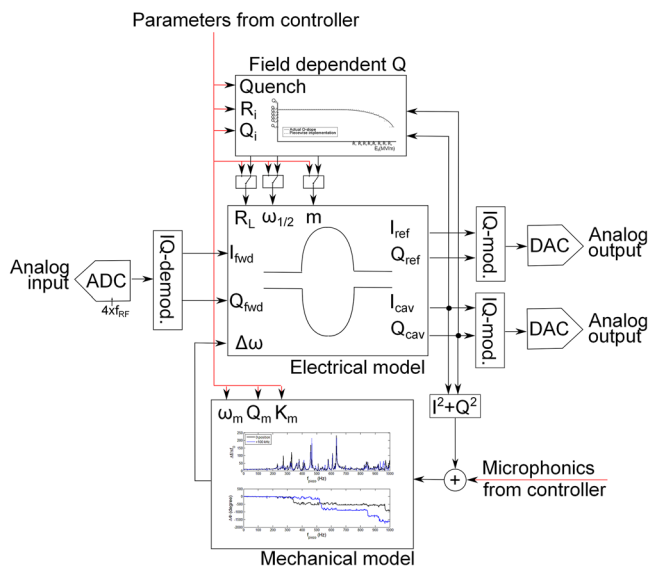


FIG. 2. Block diagram of the implemented system.

to set a high voltage until the button “Thermal Recovery” is pressed by the operator.

B. Q-dependent field

Real superconducting cavities have a field dependent Q_0 . At high fields, the quality factor shows a degradation, the so-called Q-slope, which can be a limit to high gradients.¹⁶ In order to emulate this behavior or any other field dependence, a piecewise curve can be implemented (Fig. 3). The operator can divide the cavity voltage in up to nine regions (this number can be easily increased if needed) and then define the Q_0 for those regions.

The Windows controller sends this information to the FPGA where a selector is implemented. This component uses the amplitude of the cavity voltage and the implemented look-up table to decide in real time in which region it lies and sends the corresponding parameters to the cavity model block. It also sends this information back to the controller to show the new theoretical parameters of the cavity in the GUI.

C. Mechanical response

A full cavity unit composed of the superconducting cavity, the helium vessel, and the tuner forms a mechanical structure with characteristic vibration eigenmodes. When one or several of these eigenmodes are excited, the mechanical vibration of the system changes the geometry of the cavity which leads to a shift of the resonant frequency. This vibration can be excited by two independent mechanisms: the Lorentz-force pressure made by the electromagnetic field inside the cavity and microphonics caused by helium pressure fluctuations, deterministic narrow band noise sources as vacuum pumps, stochastic background noise, etc. The eigenmodes, independent of the mechanism causing them, can be described by three parameters: the resonance frequency, the quality factor, and the coupling factor.⁸ For the Lorentz force case, the detuning introduced by one eigenmode is described by

$$\frac{d}{dt} \begin{pmatrix} \Delta\omega_m(t) \\ \Delta\dot{\omega}_m(t) \end{pmatrix} = \begin{pmatrix} 0 & 1 \\ -\omega_m^2 - \frac{\omega_m}{Q_m} & 0 \end{pmatrix} \begin{pmatrix} \Delta\omega_m(t) \\ \Delta\dot{\omega}_m(t) \end{pmatrix} + \begin{pmatrix} 0 \\ -K_m\omega_m^2 \end{pmatrix} E_{cav}^2, \quad (7)$$

where $\Delta\omega_m(t)$ is the detuning, ω_m , Q_m , and K_m are, respectively, the natural frequency, the quality factor, and the coupling factor of the driven force of the eigenmode, and E_{cav} is the electric field in the cavity. The microphonics mechanism is described by a similar equation where the electric field is replaced by the voltage of the piezo elements of the mechanical tuner.¹⁷

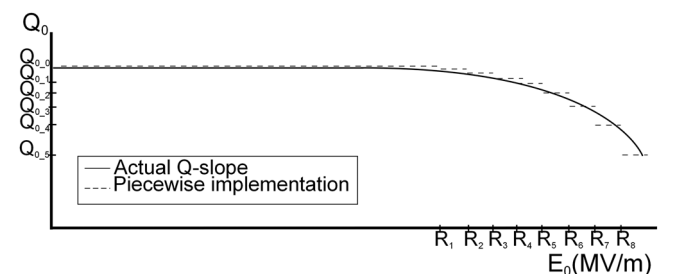


FIG. 3. Piecewise implementation of the Q-slope.

After a proper discretization, Eq. (7) is implemented in the FPGA using five blocks in parallel to simulate five different mechanical modes. The operator can introduce the necessary parameters in the graphical interface and choose which input is fed to the mechanical modes: the squared amplitude of the voltage in the cavity, a signal coming from the Windows controller with simulated microphonics, or the sum of both of them.

V. VALIDATION OF THE MODELING

A. Results for the transmitted voltage

In order to test the implementation of the cavity model, an RF signal generator was used to send a pulsed 25 MHz signal to the input of the analog adapter module. A second signal generator, synchronized with the first one, was used to generate the external 100 MHz clock source, and finally, the two analog outputs were connected to an oscilloscope.

First the V_{cav}^r and V_{cav}^i were chosen to be sent to the scope in order to check the temporal behavior of the transmitted voltage. After scanning the phase of the clock source to maximize V_{cav}^r and setting the proper digital shift for each case, the values for T_{fall} , defined as $2Q_L/\omega_0$, and the values of $V_{\text{cav}}^{\text{max}}$ without detuning, defined as $R_L\omega_{1/2}\frac{I_{\text{amp}}}{m}$, shown in Table I, are found. It can be seen that the virtual cavity's parameters are close to the theoretical ones calculated by the operator's GUI. Figure 4 compares the output extracted from the scope for the two first cases in Table I using a 500 ms pulse input with the theoretical response. It can be seen that there is a good match between the virtual cavity's output and the theoretical prediction.

TABLE I. Measured and theoretical fall time and maximum voltage without detuning as a function of Q_{ext} for $Q_0 = 5 \times 10^{10}$, $r/Q = 1000 \Omega$, $\Delta f = 0$ Hz, and $f_{\text{RF}} = 1.3$ GHz.

Q_{ext}	T_{fall}		$V_{\text{cav}}^{\text{max}}$	
	Meas.	Theo.	Meas. (MV)	Theo. (MV)
5×10^6	1.13 ms	1.22 ms	2.66	2.68
5×10^7	12.0 ms	12.23 ms	8.22	8.48
5×10^8	117 ms	121.2 ms	25.46	26.57
5×10^{10}	5.9 s	6.121 s	66.84	68.04

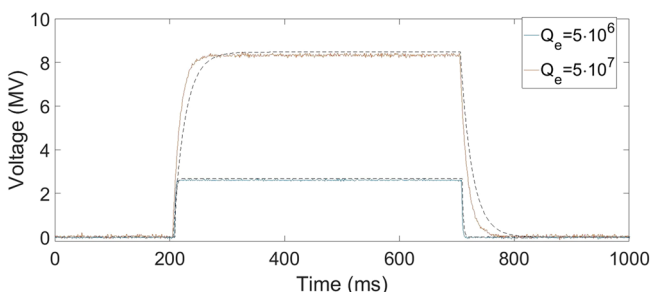


FIG. 4. Oscilloscope's readouts of the V_{cav}^r component for the first two parameters from Table I using a 500 ms pulse input signal (solid lines) versus the theoretical response (dashed lines).

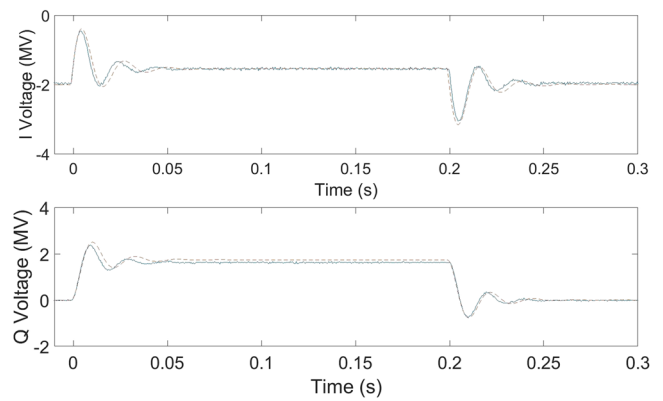


FIG. 5. Oscilloscope's readouts of V_{cav}^r (upper plot) and V_{cav}^i (lower plot) components for $Q_0 = 5 \times 10^{10}$, $Q_{\text{ext}} = 5 \times 10^7$, $r/Q = 1000 \Omega$, $f_{\text{RF}} = 1.3$ GHz, and $\Delta f = 50$ Hz using a 200 ms pulse input signal (solid lines) compared with the theoretical results (dashed lines).

In order to check the behavior of the virtual cavity with a predefined detuning, a detuning value of 50 Hz was applied. Figure 5 shows the results taken from the oscilloscope for V_{cav}^r and V_{cav}^i compared with the theoretical ones.

Finally, to check that the IQ modulation works properly, the transmitted voltage was sent to one of the analog outputs. The result is a 25 MHz signal modulated by V_{cav}^r and V_{cav}^i , as it is seen in Fig. 6.

B. Results for the reflected voltage

The behavior of the reflected voltage depends on the coupling¹⁸ defined as $\beta = \frac{Q_0}{Q_{\text{ext}}}$. To test the performance of the virtual cavity, the IQ-modulated reflected voltage was sent to the second output of the analog adapter module:

- When the cavity is critically coupled ($\beta = 1$), the reflected voltage presents two equal spikes at the beginning and the end of the pulse and in between settles to zero (Fig. 7).
- When the cavity is over-coupled ($\beta > 1$), after the first spike, the reflected voltage presents a zero-crossing and the final spike is higher than the first one (Fig. 8).

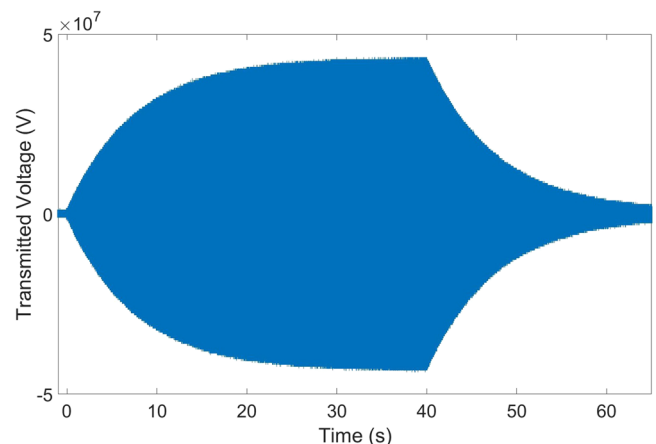


FIG. 6. Transmitted voltage for $Q_0 = 5 \times 10^{10}$, $Q_{\text{ext}} = 5 \times 10^{10}$, $r/Q = 1000 \Omega$, $f_{\text{RF}} = 1.3$ GHz, $\Delta f = 0$ Hz, and a pulse length of 30 s. The frequency of the signal is 25 MHz.

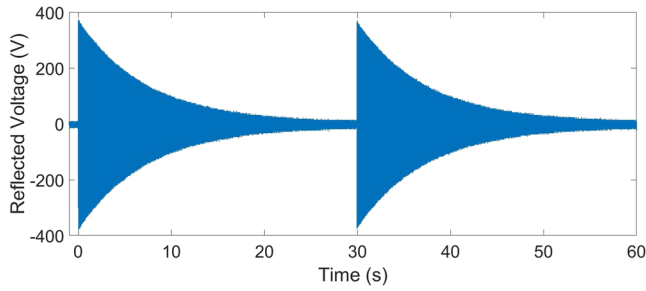


FIG. 7. Reflected voltage with $\beta = 1$.

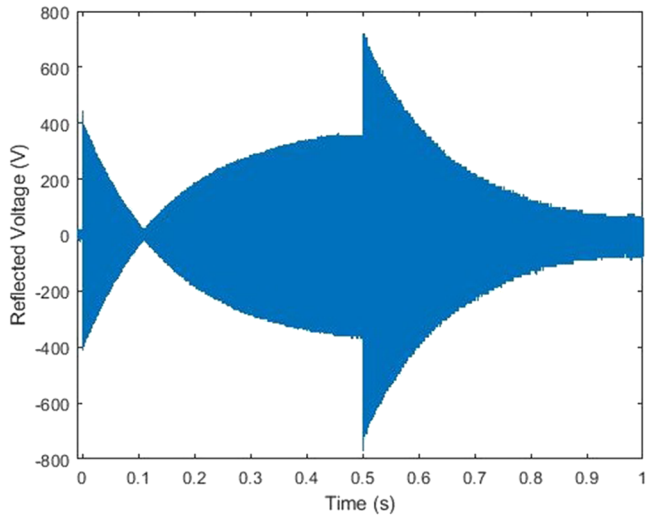


FIG. 8. Reflected voltage with $\beta = 100$.

- When the cavity is under-coupled, there is no zero-crossing after the first spike. The final spike, which is lower than the initial one, equals the steady state reflected voltage when $\beta = 1/3$ (Fig. 9). With $\beta < 1/3$, there is a step down when the pulse ends.

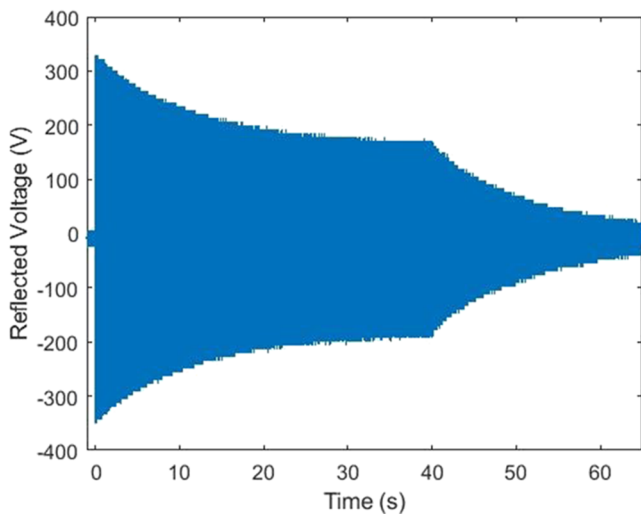


FIG. 9. Reflected voltage with $\beta = 1/3$.

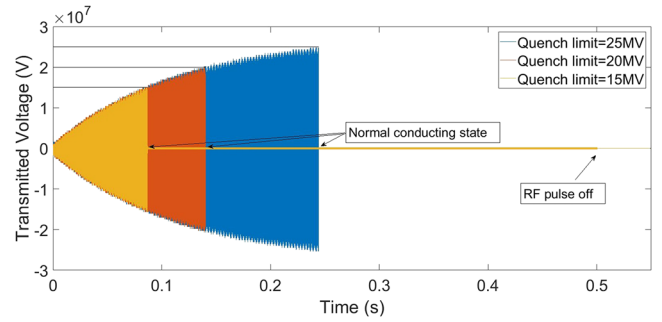


FIG. 10. Quench response for three different limits of the cavity's voltage (15, 20, and 25 MV) with a 500 ms RF pulse input.

C. Results for the quench

The correct functioning of the quench feature has been checked setting different cavity voltage limits in the controller for a given set of cavity's parameters. Figure 10 shows the quench behavior for a cavity with $Q_0 = 5 \times 10^{10}$, $Q_{ext} = 5 \times 10^8$, $r/Q = 1000 \Omega$, $f_{RF} = 1.3$ GHz. It can be seen that when the cavity voltage reaches the limit set by the user, it drops drastically to that of a normal conducting cavity.

D. Results for the Q-dependent field

In order to test the correct behavior of this feature (Subsection IV B), the exponential decay curve of the cavity voltage when the input is switched off is analyzed.¹⁹ Figure 11 shows this curve for a cavity with $Q_{ext} = 5 \times 10^8$, $r/Q = 1000 \Omega$, $f_{RF} = 1.3$ GHz and three regions for Q_0 : 5×10^{10} below 6 MV, 1×10^9 between 6 MV and 11 MV, and 1×10^8 above. By calculating the slope of the natural logarithm of the decay curve at the three different regions, the half bandwidth of the cavity can be found. Table II shows the measured half bandwidths compared to the theoretical ones.

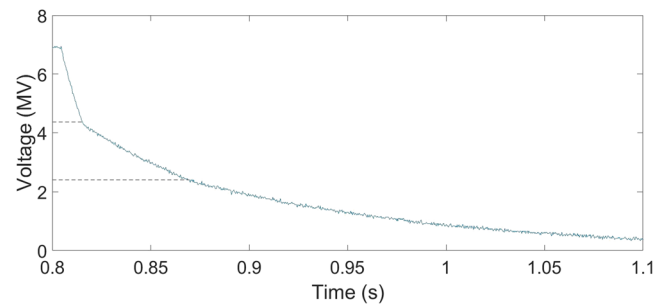


FIG. 11. Decay curve of a cavity with three Q-slope regions after switching off the input.

TABLE II. Measured and theoretical half bandwidths of the virtual cavity output with three different Q-regions.

	$\omega_{1/2}$	
	Meas. (rad/s)	Theo. (rad/s)
$V_{cav} > 11$ MV	50.508	49.009
6 MV $< V_{cav} < 11$ MV	12.753	12.252
$V_{cav} < 6$ MV	8.311	8.5765

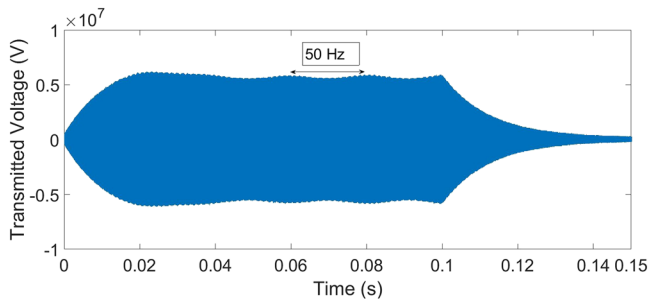


FIG. 12. The effect of the Lorentz force detuning coupled with a 50 Hz mechanical mode in the amplitude in a cavity with $Q_0 = 5 \times 10^{10}$, $Q_{ext} = 5 \times 10^7$, and $f_{RF} = 1.3$ GHz.

E. Results for the mechanical response

First the Lorentz force driven mechanical detuning was checked. Figure 12 shows the effect of a single mechanical mode of $f_m = 50$ Hz, $Q_m = 300$, and $K_m = 0.9$ on the amplitude of a cavity driven by a 100 ms pulse. It can be seen how the amplitude of the voltage in the cavity is modulated by the 50 Hz detuning signal.

The mechanical response driven by microphonics was tested using a step signal as the input of the mechanical modes, and the cavity electrical and mechanical parameters were set to mimic the behavior of the bERLinPro photoinjector.²⁰ In order to compare the results of the virtual cavity with the results of the real cavity, the same setup was used: the virtual cavity was connected to a Phase-Locked Loop (PLL) and the cavity detuning was plotted in an oscilloscope.

It is worth mentioning that this step-wise microphonics simulates a hit received by the cavity due to slug flow in the cryogenic plant,²¹ as has been observed in the SRF photoinjector for bERLinPro.²² Figure 13 shows the detuning of the virtual cavity configured as the bERLinPro photoinjector when receiving step-wise microphonics. This can be compared to the beating seen in the real photoinjector due to the slug flow, as it is shown in Fig. 14. Figure 15 shows the Fourier transform of the detuning of the virtual cavity, where

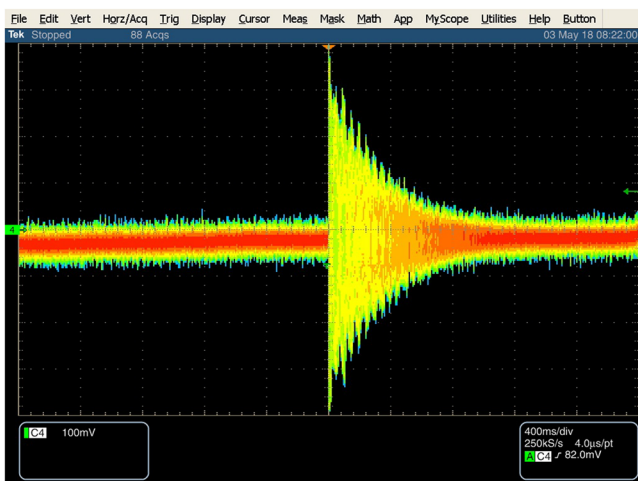


FIG. 13. Cavity detuning measured using a PLL of the virtual cavity configured as the bERLinPro photoinjector when receiving step-wise microphonics.

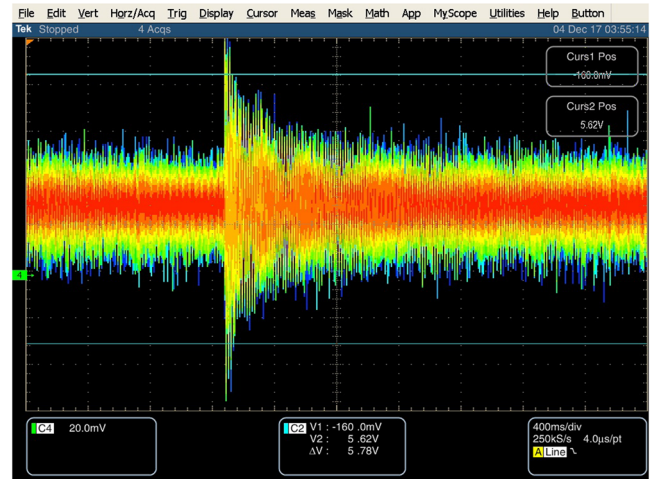


FIG. 14. Beating in the SRF Photoinjector measured at HZB due to the slug flow.

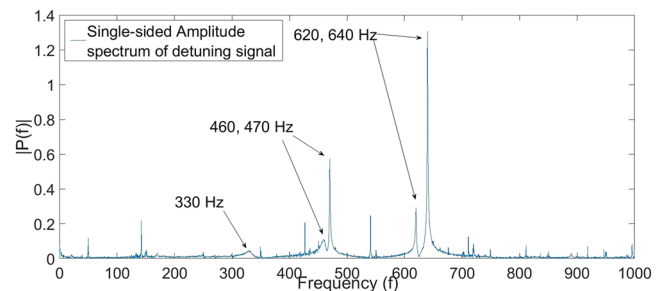


FIG. 15. Fourier transform of the detuning of the virtual cavity configured as a bERLinPro photoinjector.

the mechanical modes introduced through the virtual cavity's user interface can be clearly seen.

VI. LIMITATIONS OF THE HARDWARE

The main limitation of the presented virtual cavity is that as an FPGA is used for the implementation, fixed point representation is the most suitable way to manipulate data. Thus, some quantization errors are introduced in the cavity parameters' data representation and therefore into the virtual cavity's dynamics. In this sense, the parameter with the biggest impact in the cavity's dynamics is $\omega_{1/2}$, whose bit representation has been chosen to allow up to 24 krad/s half bandwidth with a precision of around 3 mrad/s. This means that, for example, at $f_{RF} = 1.3$ GHz, the minimum Q_L is around 1.75×10^5 and the maximum is around 5×10^{11} . It also means that the closer the Q_L is to the upper limit, the bigger the quantization error is (around 6% at $f_{RF} = 1.3$ GHz and $Q_L = 5 \times 10^{11}$).

The utilization of a rather old FPGA also has a direct impact on the features that can be implemented. For instance, the number of multiplier blocks limits the number of mechanical eigenmodes to a maximum of five. It is planned to migrate the project to a newer hardware²³ with a more powerful FPGA that will allow us to implement more mechanical modes, to emulate the effect of the beam loading, implement more passband modes, etc.

The quench response can also be improved to approximate better the real behavior, where the drop of Q_0 follows a decay curve which takes few milliseconds, and the resonant frequency ω_0 is shifted due to the difference between the penetration depth in the superconducting state and the skin effect in the normal conducting state. This means that after a quench, the values of $\omega_{1/2}$ and $\Delta\omega$ have to be fed into the cavity model from a look-up table.

Regarding the microphonics, currently only two possible types are implemented: white noise, which is implemented using a predefined Labview block that allows to choose between uniformly or Gaussian-distributed pseudorandom patterns,²⁴ and step-wise microphonics. It is planned to include the possibility of choosing real recorded microphonics to emulate more realistic situations.

Finally the sampling speeds of the ADCs and DACs make it compulsory to use down- and up-converters to shift the frequency of the signals from RF to the intermediate frequency and vice versa.

VII. EXAMPLES OF APPLICATIONS

In order to use the virtual cavity to debug the actual control hardware and algorithms, the virtual cavity has been connected to an up/down converter to generate a 1.3 GHz signal. Currently it is being used to debug the utilization of a Kalman filter for the cavity detuning estimation.²⁵ For such a purpose, five mechanical modes have been selected driven by step-type microphonics, and the up-converted output has been connected to the μ TCA chassis that will be used for the bERLinPro LLRF (low level RF) control.²⁰

The virtual cavity is not only limited to applications in LLRF control algorithms debugging but can be used for a wider range of debugging. For instance, its quench feature has been used to debug a quench detection software that was later used in a quadrupole resonator.²⁶

Due to its flexibility and the wide range of the parameters, the virtual cavity becomes a very useful tool as well for teaching superconducting radio-frequency science and technology. For example, the graphical user interface can be modified to hide some parameters to allow the students to measure the loaded quality factor through the decay time, the Q versus field curve, etc.

VIII. CONCLUSIONS AND FURTHER DEVELOPMENTS

The flexibility of the presented virtual cavity allows the emulation of the electrical model of several types of superconducting cavities, together with some advanced features like quenching, field dependent Q, Lorentz force detuning, and mechanical modes driven by the Lorentz force or by external microphonics. Currently it is being used to debug LLRF control algorithms for the bERLinPro Energy Recovery Linac and BESSY-VSR and it is planned to be used in the Accelerator Physics program of the University of Siegen. It is also foreseen to be used to test the LLRF operation including piezo controls,²⁷ which will need to implement the behavior of the piezo elements of the cavity tuners coupled to its mechanical

response. The microphonics source in the Windows controller is also planned to be extended to allow the possibility of sending not only step-type perturbations or white noise but, for example, real microphonics recorded in an actual cavity.

As the hardware used for the implementation is based on commercial, off-the-shelf hardware, the distribution of the virtual cavity can be done by sharing the LabView project, enabling the development and debugging of control algorithms for superconducting cavities in facilities without the necessary ancillary systems. In order to make the virtual cavity more compact and to update it with a more powerful FPGA, it is planned to migrate the project to a FlexRIO controller.²³

¹D. Boussard and T. Linnecar, "The LHC superconducting RF system," LHC Project Report 316, CERN, Geneva, Switzerland, 1999.

²W. Singer, X. Singer, A. Brinkmann, J. Iversen, A. Matheisen, A. Navitski, Y. Tamashevich, P. Michelato, and L. Monaco, "Superconducting cavity material for the European XFEL," *Supercond. Sci. Technol.* **28**, 085014 (2015), IOP Publishing Ltd.

³J. Galayda, "The new LCLS-II project: Status and challenges," in *Proceedings, 27th Linear Accelerator Conference, LINAC2014*, Geneva, Switzerland, August 31–September 5, 2014, <http://www.jacow.org>, p. TUIOA04.

⁴A. Arnold, H. Buettig, D. Janssen, T. Kamps, G. Klemz, W. Lehmann, U. Lehnert, D. Lipka, F. Marhauser, P. Michel, K. Moeller, P. Murcek, C. Schneider, R. Schurig, F. Staufienbiel, J. Stephan, J. Teichert, V. Volkov, I. Will, and R. Xiang, "Development of a superconducting radio frequency photoelectron injector," *Nucl. Instrum. Methods Phys. Res., Sect. A* **577**, 440–454 (2007).

⁵F. Schlander, K. Aulenbacher, R. Heine, D. Simon, and T. Stengler, "1.3 GHz SRF cryomodules for the Mainz energy-recovering superconducting accelerator MESA," in *Proceedings, 6th International Particle Accelerator Conference (IPAC 2015)*, Richmond, Virginia, USA, May 3–8, 2015, <http://www.jacow.org>, p. WEPMA041.

⁶A. Velez, H. W. Glock, F. K. Gloekner, B. Hall, A. Neumann, E. Sharples, P. Schnizer, A. Tsakanian, and J. Knobloch, "The SRF module developments for BESSY-VSR," in *Proceedings, 6th International Particle Accelerator Conference (IPAC 2017)*, Copenhagen, Denmark, 2017.

⁷A. Neumann, W. Anders, A. Burril, A. Frahm, H. W. Glock, J. Knobloch, O. Kugeler, G. Ciovati, W. Clemens, C. Dreyfuss, D. Forehand, T. Harris, P. Kneisel, R. Overton, L. Turlington, K. Brackebusch, T. Galek, J. Heller, and U. van Rienen, "Update on SRF cavity design, production and testing for BERLinPro," in *Proceedings, 17th International Conference on RF Superconductivity (SRF2015)*, Whistler, Canada, September 13–18, 2015, <http://www.jacow.org>, p. THPB026.

⁸T. Czarski, K. T. Pozniak, R. S. Romaniuk, and S. Simrock, "TESLA cavity modeling and digital implementation in FPGA technology for control system development," *Nucl. Instrum. Methods Phys. Res., Sect. A* **556**, 565–576 (2006).

⁹A. Grassellino, J. K. Keung, and F. M. Newcomer, "FPGA based ILC cavity simulator," in *Proceedings of PAC07*, Albuquerque, New Mexico, USA, 2007, <http://www.jacow.org>, p. 632.

¹⁰R. Kleindienst, A. Burrill, J. Knobloch, and O. Kugeler, "Commissioning results of the HZB quadrupole resonator," in *Proceedings, 17th International Conference on RF Superconductivity (SRF2015)*, Whistler, Canada, September 13–18, 2015, <http://www.jacow.org>, CERN-ACC-2015-0114, p. WEA1A04.

¹¹T. Schilcher, "Vector sum control of pulsed accelerating fields in Lorentz force detuned superconducting cavities," Ph.D. thesis, Hamburg University, 1998.

¹²See <http://www.ni.com/pdf/manuals/375175c.pdf> for NI PXIe-1071.

¹³See <http://www.ni.com/pdf/manuals/373716b.pdf> for NI PXIe-8135.

¹⁴See <http://www.ni.com/pdf/manuals/373047b.pdf> for PXIe-7966.

¹⁵See <http://www.ni.com/pdf/manuals/372968a.pdf> for NI-5781.

¹⁶J. Knobloch, R. L. Geng, M. Liepe, and H. Padamsee, "High-field QSlope in superconducting cavities due to magnetic field enhancement at grain boundaries," in *Proceedings of the 9th Workshop on RF Superconductivity*, Santa Fe, USA, 1999.

¹⁷A. Neumann, W. Anders, O. Kugeler, and J. Knobloch, "Analysis and active compensation of microphonics in continuous wave narrow-bandwidth superconducting cavities," *Phys. Rev. Spec. Top.–Accel. Beams* **13**, 082001 (2010).

- ¹⁸T. Powers, *Theory and Practice of Cavity RF Test Systems* (U.S. Department of Energy Office of Energy Research, 2006).
- ¹⁹H. Padamsee, J. Knobloch, and T. Hays, *RF Superconductivity for Accelerators* (Wiley-VCH, 2008).
- ²⁰P. Echevarria, J. Knobloch, O. Kugeler, A. Neumann, K. Przygoda, and A. Ushakov, "First LLRF tests of BERLinPro gun cavity prototype," in *Proceedings of International Particle Accelerator Conference (IPAC'16), Busan, Korea, May 8–13, 2016*, International Particle Accelerator Conference No. 7, Geneva, Switzerland, 2016, <http://www.jacow.org>, pp. 1831–1834.
- ²¹G. Celata, M. Cumo, D. Dossevi, R. Jilisen, S. Saha, and G. Zummo, "Flow pattern analysis of flow boiling inside a 0.48 mm microtube," *Int. J. Therm. Sci.* **58**, 1–8 (2012).
- ²²A. Neumann, D. Boehlick, M. Buerger, P. Echevarria, A. Frahm, H.-W. Glock, F. Goebel, S. Heling, K. Janke, A. Jankowiak, T. Kamps, S. Klauke, G. Klemz, J. Knobloch, G. Kourkafas, J. Kuehn, O. Kugeler, N. Leuschner, N. Ohm, E. Panofski, H. Ploetz, S. Rotterdam, M. A. H. Schmeisser, M. Schuster, H. Stein, Y. Tamashevich, J. Ullrich, A. Ushakov, and J. Voelker, "The bERLinPro SRF photoinjector system—from first RF commissioning to first beam," in *Proceedings of International Particle Accelerator Conference (IPAC'18), Vancouver, Canada, 29 April–4 May 2018*.
- ²³See <http://www.ni.com/de-de/support/model.ni-7935.html> for NI-7935.
- ²⁴See http://zone.ni.com/reference/en-xx/help/371599n-01/lvfpga/fpga-white_noise/ for NI White Noise.
- ²⁵A. Ushakov, P. Echevarria, and A. Neumann, "Detuning compensation in SC cavities using Kalman filters," in *Proceedings of International Particle Accelerator Conference (IPAC'17), Copenhagen, Denmark, 14–19 May 2017*, International Particle Accelerator Conference No. 8, Geneva, Switzerland, 2017, <http://www.jacow.org>, pp. 3938–3940.
- ²⁶F. Kramer, "Messung des kritischen magnetfelds von supraleitenden proben in hochfrequenzfeldern," B.Sc. thesis, Universität Siegen, 2017.
- ²⁷K. Przygoda, R. Rybaniec, V. Ayvazyan, H. Schlarb, C. Schmidt, J. Sekutowicz, and P. Echevarria, "Experience with single cavity and piezo controls for short, long pulse and CW operation," in *Proceedings of International Particle Accelerator Conference (IPAC'17), Copenhagen, Denmark, 14–19 May 2017*, International Particle Accelerator Conference No. 8, Geneva, Switzerland, 2017, <http://www.jacow.org>, pp. 3966–3968.